Zhai et al. Nanoscale Research Letters (2017) 12:496
DOI 10.1186/s11671-017-2273-8

Nanoscale Research Letters

NANO EXPRESS Open Access

The Effects of Li/Nb Ratio on the Preparation and Photocatalytic Performance of Li-Nb-O Compounds

Haifa Zhai[1,2*], Hairui Liu[1], Hongjing Li[1], Liuyang Zheng[1], Chunjie Hu[1], Zhao Wang[1], Jingjing Qi[1] and Jien Yang[1]

Abstract

The effects of Li/Nb ratio on the preparation of Li-Nb-O compounds by a hydrothermal method were studied deeply. Li/Nb ratio has a great impact on the formation of $LiNbO_3$; the ratio smaller than 3:1 is beneficial to the formation of $LiNbO_3$, while larger than 3:1, forms no $LiNbO_3$ at all and the morphology and chemical bond of Nb_2O_5 raw material are totally modified by Li ions. The reason can be attributed to the large content of LiOH, which is beneficial to form Li_3NbO_4 not $LiNbO_3$, and also, even if $LiNbO_3$ particle locally forms, it is easily dissolved in LiOH solution with strong alkalinity. Pure $LiNb_3O_8$ powders are obtained with two absolutely opposite Li/Nb ratios: 8:1 and 1:3; the former shows a unique porous and hollow structure, quite different from the particle aggregation (the latter shows). Compared with Li/Nb = 1:3, the 4.2 times higher photocatalytic performance of $LiNb_3O_8$ (Li/Nb = 8:1) are observed and it can be attributed to the unique porous and hollow structure, which provides a high density of active sites for the degradation of MB. Compared to $LiNbO_3$, the improved photocatalytic performance of $LiNb_3O_8$ can be attributed to its layered structure type with the reduced symmetry enhancing the separation of electrons and holes.

Keywords: Lithium Niobate, Hydrothermal, Porous Materials, Photocatalysis

Background

Niobium compounds, a very versatile group of materials, including niobium oxides, alkali niobates, and columbite niobates, exhibit many interesting physical properties and have been widely studied in many fields, such as catalysis [1–3], memristors [4], dye-sensitized solar cells [5], optical devices, and others [6, 7]. $LiNbO_3$, as one of the most famous alkali niobates, presents prominent properties such as electro-optical and nonlinear optical behaviors, pyroelectricity, and piezoelectricity, and it is mainly used as optical modulators, waveguides, acoustic wave transducers, et al. in optical devices.

For environmental remediation and clean energy applications, niobates, such as (Na, K)NbO_3 [8], $BiNbO_4$ [9], $LiNbO_3$ [10], and $LiNb_3O_8$ [11], have been deeply investigated, owing to their special distorted [NbO_6] octahedral structures which favor a possible delocalization of charge carriers [12]. Secondly, the conduction bands consisting of Nb4d orbitals located at a more negative state of redox potential of $H+/H_2$ promote the separation and transfer of photo-induced charge carriers and result in high photocatalytic activities [13]. Among these materials, $LiNb_3O_8$ displays unique performances. As a novel lithium-ion battery (LIB) anode material, the theoretical capacity of $LiNb_3O_8$ is 389 mAh/g assuming two-electron transfers ($Nb^{5+} \rightarrow Nb^{3+}$), larger than many other anode materials, such as $Li_4Ti_5O_{12}$ [14, 15]. Used for supercapacitor devices, $LiNb_3O_8$ nanoflakes show excellent cycle stability with negligible specific capacitance decrease even after 15,000 cycles [16]. Also, it is used as an efficient photocatalyst in the applications of hydrogen generation and degradation of organic pollutants. Pure $LiNb_3O_8$ is a highly active UV-photocatalyst for water reduction producing 83.87 μmol of hydrogen in 1 h, and it does not produce hydrogen under visible-light irradiation due to its large band gap (i.e., 3.9 eV) and inability to absorb visible light [17, 18]. $LiNb_3O_8$ nanoflakes show fast decolorization of

* Correspondence: haifazhai@126.com
[1]Henan Key Laboratory of Photovoltaic Materials, College of Physics and Materials Science, Henan Normal University, Xinxiang 453007, People's Republic of China
[2]National Laboratory of Solid State Microstructures, Nanjing University, Nanjing 210093, People's Republic of China

toluidine blue O (TBO) dye under UV light compared to commercial TiO_2 powders [13].

At most time, the appearance of $LiNb_3O_8$ is recognized as an impurity phase during the preparation of $LiNbO_3$, especially in film samples, owing to high annealing temperature or inhomogeneous distribution of Li element in precursors [19, 20]. Due to the difficulty to prepare a pure phase, $LiNb_3O_8$ has been rarely studied, while for $LiNbO_3$ powders, the preparation technologies are various, such as sol-gel [19], hydrothermal [21], and laser irradiation methods [22]. Hydrothermal method is widely used to synthesize nanomaterials with advantages such as low temperature, environmental friendliness, and homogenous particle-size distribution, which can efficiently avoid the variation of Li/Nb molar ratio without going through high temperatures. As for hydrothermal method, the parameters of reaction temperature, raw material ratio, and holding time play important roles in determining the as-obtained materials, while the research of Li/Nb ratio much larger than 1:1 in the preparation of Li-Nb-O compounds has not been reported before.

In this paper, the effects of Li/Nb ratio on the preparation of Li-Nb-O compounds by a hydrothermal method were studied deeply. A series of analytical techniques were used to characterize the crystallinity, morphology, and chemical composition of the Li-Nb-O samples, especially the changes before and after the hydrothermal reaction. Pure $LiNb_3O_8$ and $LiNbO_3$ photocatalysts were prepared, and the photocatalytic performance was studied with the effect of Li/Nb ratio in raw materials.

Methods

The preparation of Li-Nb-O compounds was carried out by the hydrothermal method using lithium hydroxide monohydrate ($LiOH{\cdot}H_2O$; Aladdin, ACS, ≥ 98.0%) and niobium pentaoxide (Nb_2O_5; Aladdin, AR, 99.9%) as starting materials. Firstly, 3.5 mmol of Nb_2O_5 was dispersed into 35 ml deionized water with a certain amount of $LiOH{\cdot}H_2O$ under magnetic stirring. The mole ratios of Li:Nb are 1:3, 1:1, 2:1, 3:1, 4:1, 5:1, 6:1, 7:1, and 8:1; as the results of the samples prepared with ratios of 4:1, 5:1, 6:1, and 7:1 are similar, only the ratios of Li:Nb = 4:1 and 7:1 are shown below. The suspension solutions were put into 50-mL Teflon-lined hydrothermal synthesis autoclave reactors and maintained at 260 °C for 24 h, then cooled down naturally to room temperature. The as-obtained powders were then washed with deionized water and ethanol for several times and dried at 60 °C. Finally, the products were calcined at various temperatures from 500 to 800 °C for 2 h with a ramp rate of 5 °C/min.

The X-ray diffraction (XRD) patterns were recorded using a Bruker D8 Discover diffractometer with Cu *Kα* radiation (40 kV, 40 mA). The morphologies of the samples were characterized by field emission scanning electron microscope (FESEM; JSM-6700F). Chemical bonds were analyzed by Fourier-transformed infrared spectroscopy (FTIR) in the range of 2000–650 cm^{-1}. X-ray photoelectron spectroscopy (XPS) analysis was performed on a Thermo-Fisher Escalab 250Xi instrument to characterize the chemical component of Li-Nb-O compounds. The specific surface area was measured on a surface area apparatus (Micromeritics ASAP 2460) at 77 K by N_2 adsorption/desorption method (BET method). The photoluminescence (PL) spectra were detected using an F-280 fluorescence spectrophotometer with an excitation wavelength of 320 nm.

To evaluate the photocatalytic performance of Li-Nb-O compounds, the degradation of methylene blue (MB) aqueous solution (5 mg/L) was carried out under irradiation of a 500 W Hg lamp at a natural pH value. Fifty milligrams of powders were dispersed into 50 mL of MB aqueous solution. Before the irradiation, the suspension was stirred in dark for 1 h to achieve adsorption equilibrium. Then, the suspension was irradiated by the Hg lamp. The concentration of residual MB was analyzed with an interval of 30 min using an ultraviolet-visible near-infrared (UV-vis-NIR) spectrophotometer at 665 nm.

Results and Discussion

The XRD patterns of the products obtained after hydrothermal reaction with different Li/Nb mole ratios are shown in Fig. 1. It is obvious that pure $LiNbO_3$ phase (JCPDF, No. 20-0631) is obtained with Li:Nb = 2:1. For the ratio of Li/Nb smaller than 2:1, such as 1:1 or 1:3, the main phase is still $LiNbO_3$, accompanied with the residual of Nb_2O_5 (JCPDF, No. 37-1468), which means that the Li content is not sufficient to fully react with Nb_2O_5 to form $LiNbO_3$. When we increase the Li content largely, an amazing phenomenon occurs: there is no $LiNbO_3$ formed at all after the hydrothermal reaction, as

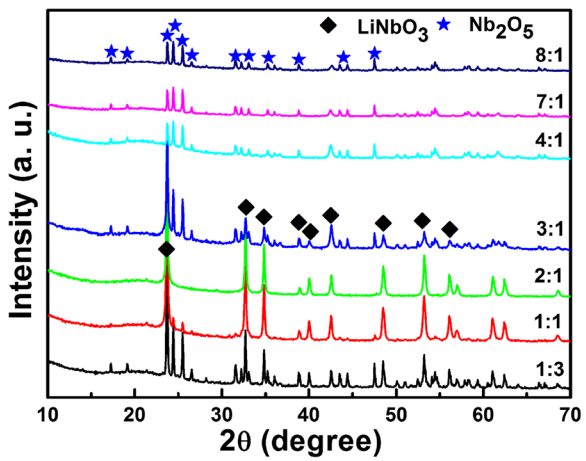

Fig. 1 XRD patterns of the Li-Nb-O powders obtained after hydrothermal reaction with different Li/Nb mole ratios

clearly shown in Fig. 1. When the ratio of Li/Nb is 4:1 or larger, only Nb_2O_5 phase exists in XRD patterns, no other impurities detected. Is the Li ion washed away during the washing process? Just like the former literature reported [23].

To illustrate the phase evolution when the Li/Nb ratio is large enough, the products obtained by the hydrothermal method, using Li/Nb = 8:1 as an example, are calcined at different temperatures and the XRD patterns are shown in Fig. 2. When the products are calcined at 500 and 600 °C, a new phase $LiNbO_3$ appears which proves that a Li element truly exists in the products obtained just after the hydrothermal reaction, though not detected by XRD. Also, a diffraction peak at 30.26° appears at 600 °C, which can be indexed as (410) plane of monoclinic $LiNb_3O_8$. The reaction can be described by the following Eq. (1) [24]:

$$LiNbO_3 + Nb_2O_5 \rightarrow LiNb_3O_8 \quad (1)$$

At 700 °C, the monoclinic $LiNb_3O_8$ is the predominant phase with almost negligible impurity. The pure phase of $LiNb_3O_8$ is obtained at 800 °C with all the diffraction peaks indexed to the monoclinic phase (JCPDF, No. 36-0307), a space group of P21/a, which provides a new way to prepare $LiNb_3O_8$ compounds.

FTIR test is also performed to study the phase evolution of the products with Li:Nb = 8:1, as shown in Fig. 3. The raw material Nb_2O_5 is tested as a reference. In Fig. 3, the band at 962 cm^{-1} due to the stretching vibrations of Nb = O in Nb_2O_5 is existent until 700 °C [25]. After hydrothermal reaction, no other bands detected at this range means the only niobate is still Nb_2O_5. When the calcination temperature is 500 and 600 °C, a new band

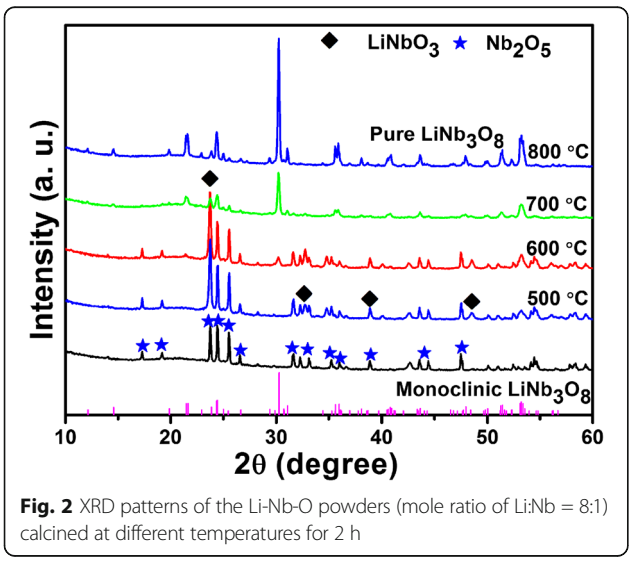

Fig. 2 XRD patterns of the Li-Nb-O powders (mole ratio of Li:Nb = 8:1) calcined at different temperatures for 2 h

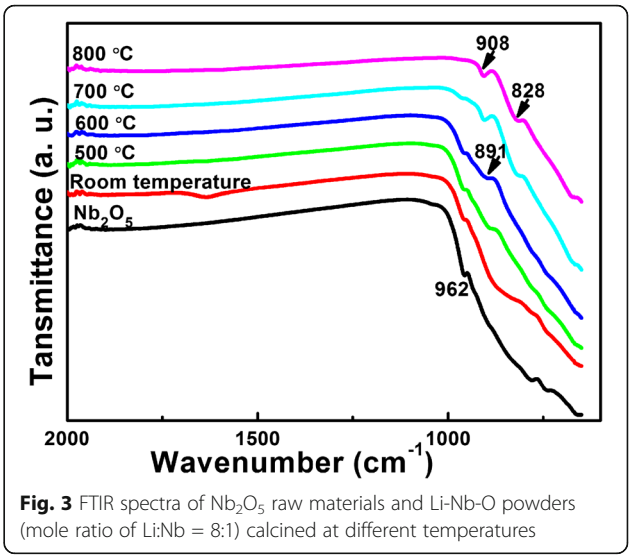

Fig. 3 FTIR spectra of Nb_2O_5 raw materials and Li-Nb-O powders (mole ratio of Li:Nb = 8:1) calcined at different temperatures

at 891 cm^{-1} appears, while disappears at 700 °C, consistent with the XRD results of the formation and reaction of $LiNbO_3$. At 700 and 800 °C, the bands at 908 and 828 cm^{-1} correspond to the formation of $LiNb_3O_8$ compounds [26, 27]. The FTIR results are well consistent with the XRD results of Fig. 2.

Based on the results, we can conclude that Li/Nb ratio has a great impact on the formation of $LiNbO_3$; the ratio smaller than 3:1 is beneficial to the formation of $LiNbO_3$, while larger than 3:1, no $LiNbO_3$ forms at all. Based on the diagram, the congruent Li content is 97.2 mol% of the Nb content for the preparation of perfect single-phase $LiNbO_3$, and the excess or deficiency of the Li content is compensated by the formation of Li_3NbO_4 or $LiNb_3O_8$ phase [28]. The large excess of LiOH is beneficial to form Li_3NbO_4 not $LiNbO_3$, while no Li_3NbO_4 phase is observed after hydrothermal reaction due to the insufficient reaction condition; even if the $LiNbO_3$ particle locally formed, it is easily dissolved in LiOH solution with strong alkalinity [29].

As discussed above, the Li element is not detected after the hydrothermal reaction without further calcination, while it truly exists in the products with Li:Nb = 8:1. For Nb_2O_5, is it still the same as the raw material after the hydrothermal reaction? The XPS test is carried out to characterize the chemical component of Nb_2O_5 raw material and the products obtained after hydrothermal reaction, as shown in Fig. 4. The difference of Nb $3d_{3/2}$ and $3d_{5/2}$ is the 2.7 eV for both samples, indicating the Nb^{5+} state in both samples without other reduced Nb oxides species [3]. The binding energies of Nb 3d shift towards the low binding-energy state after the hydrothermal reaction, about 0.5 eV difference. It means that the chemical environment of Nb changes, while no other compounds are formed. The change may

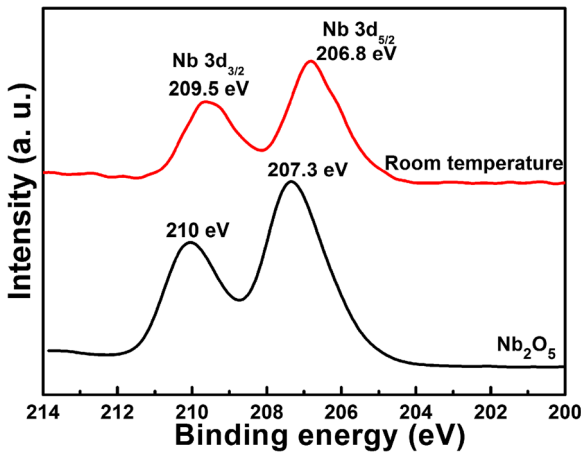

Fig. 4 XPS spectra of Nb_2O_5 raw materials and the products (mole ratio of Li:Nb = 8:1) obtained after hydrothermal method

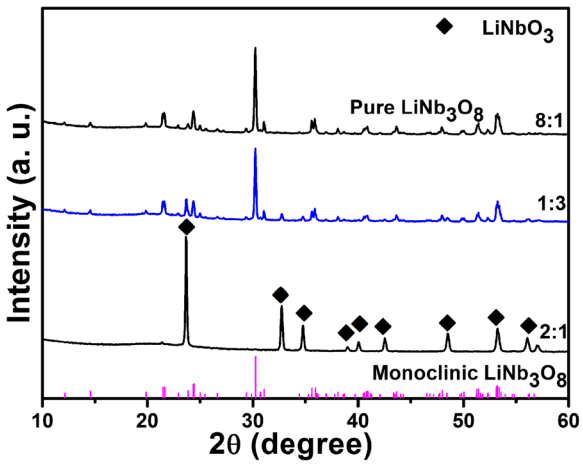

Fig. 6 XRD patterns of three typical Li/Nb ratios products calcined at 800 °C for 2 h

be due to the existence of Li ions in the product; though no obvious Li-Nb-O compound is formed, the existence of Li ions with larger iconicity has strong attraction of O ions around Nb, resulting in the chemical shift of Nb 3d binding energy.

The influence of Li ions on Nb_2O_5 is also observed in SEM images, as shown in Fig. 5. Figure 5a is the image of Nb_2O_5 raw material, with irregular shape, dense structure, and length of several micrometers. After the hydrothermal reaction, the large crystal particle is divided into small particles with the maximum size of about 200 nm, though the small particles still aggregate together. From the XRD and XPS results, we know that the small particles are still Nb_2O_5. The change of the morphology of Nb_2O_5 can be attributed to the hydrothermal condition and large content of $LiOH{\cdot}H_2O$ in raw materials.

The products obtained after hydrothermal reaction are calcined at 800 °C with different Li/Nb ratios. Hereafter, we choose three typical Li/Nb ratios as examples: 1:3, 2:1, and 8:1. The XRD patterns of the three samples are shown in Fig. 6. From the XRD results, pure $LiNbO_3$ are prepared with Li/Nb = 2:1 and has shown no change even when calcined at 800 °C. For the preparation of another Li-Nb-O compound $LiNb_3O_8$, it can be obtained with two absolutely opposite Li/Nb ratios: 8:1 and 1:3 (designated as $LiNb_3O_8$-8:1 and $LiNb_3O_8$-1:3). For other Li/Nb ratios not shown in Fig. 6, the products calcined at 800 °C result in the formation of two mixed phases: $LiNb_3O_8$ and $LiNbO_3$. Based on the XRD results, pure $LiNb_3O_8$ powders are prepared with two different Li/Nb ratios, while is there any differences between the two products?

The SEM images of the two products are displayed as Fig. 7b, c, respectively. As shown in Fig. 7, the morphology of $LiNb_3O_8$-1:3 are quite different with that of $LiNb_3O_8$-8:1. $LiNb_3O_8$-8:1 has a porous and hollow structure formed by $LiNb_3O_8$ nanoparticles with the length of several micrometers, similar as that of a honeycomb. It is quite different with the particle aggregation of solid-state reaction, as $LiNb_3O_8$-1:3 shown. The BET areas of $LiNb_3O_8$-8:1 and $LiNb_3O_8$-1:3 are 4.46 and 0.96 m^2/g, respectively, the larger surface area of the

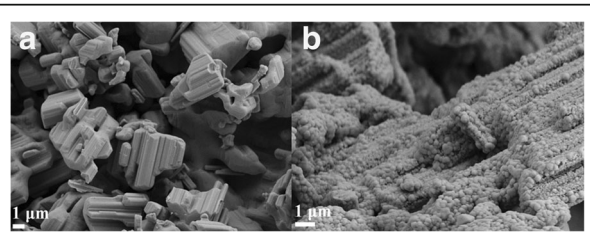

Fig. 5 SEM images of **a** Nb_2O_5 raw materials and **b** the products (mole ratio of Li:Nb = 8:1) obtained after hydrothermal method

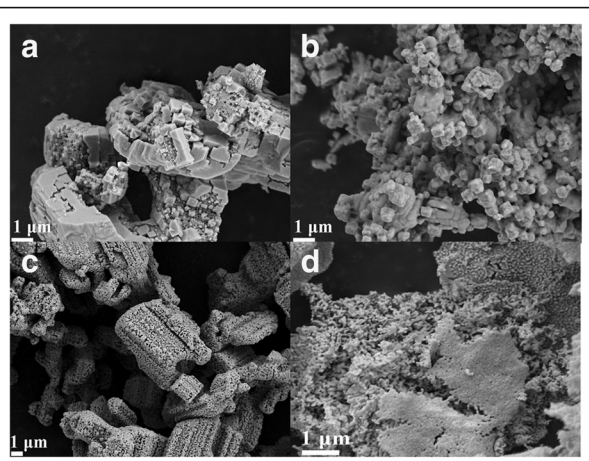

Fig. 7 SEM images of three typical Li/Nb ratios products calcined at different temperatures: **a** 2:1 at 500 °C, **b** 1:3, **c** 8:1, and **d** 2:1 at 800 °C

former results from the porous and hollow structure. The morphology difference can be attributed to the different morphologies of the reactants: for $LiNb_3O_8$-8:1, the reactant of $LiNbO_3$ is formed based on the calcinations of the products after hydrothermal reaction, the morphology of the products is shown in Fig. 5b, while for $LiNb_3O_8$-1:3, the morphology of $LiNbO_3$ obtained directly after the hydrothermal reaction is hexahedron-like, as shown in Fig. 7a [21]. The formation of the porous and hollow structure for $LiNb_3O_8$-8:1 can be attributed to the lithium volatilization during the calcinations process, which is beneficial to the formation of new $LiNb_3O_8$ particles and networks between the particles [11]. For $LiNbO_3$ calcined at 800 °C (i.e., Li/Nb = 2:1), its grain size is about 200 nm and the shape seems irregular, as shown in Fig. 7d; the BET area is about 3.91 m^2/g.

The photocatalytic performances of $LiNb_3O_8$ and $LiNbO_3$ are shown in Fig. 8. From the UV-vis absorption spectra of MB at the varied irradiation time (Fig. 8a–d), it is observed that the maximum absorption band (665 nm) becomes weak with the increase of the irradiation time. The degradation rate of MB is largely improved with the catalysts of $LiNb_3O_8$ and $LiNbO_3$ under UV light, especially for $LiNb_3O_8$-8:1, about 85% of MB degraded after 30 min irradiation, as shown in Fig. 8e. As the photo-degradation of MB using Li-Nb-O catalysts obeys the pseudo-first-order kinetics, described by the modified Langmuir-Hinshelwood kinetics mode [30], the constants of the pseudo-first-order rate (k) are calculated, displayed in Fig. 8f. The obtained first-order rate constants of MB without catalysts, $LiNb_3O_8$-1:3, $LiNbO_3$, and $LiNb_3O_8$-8:1 are 0.71×10^{-2}, 1.61×10^{-2}, 4.18×10^{-2}, and 6.73×10^{-2} min^{-1}, respectively. The higher the first-order rate constant is, the more

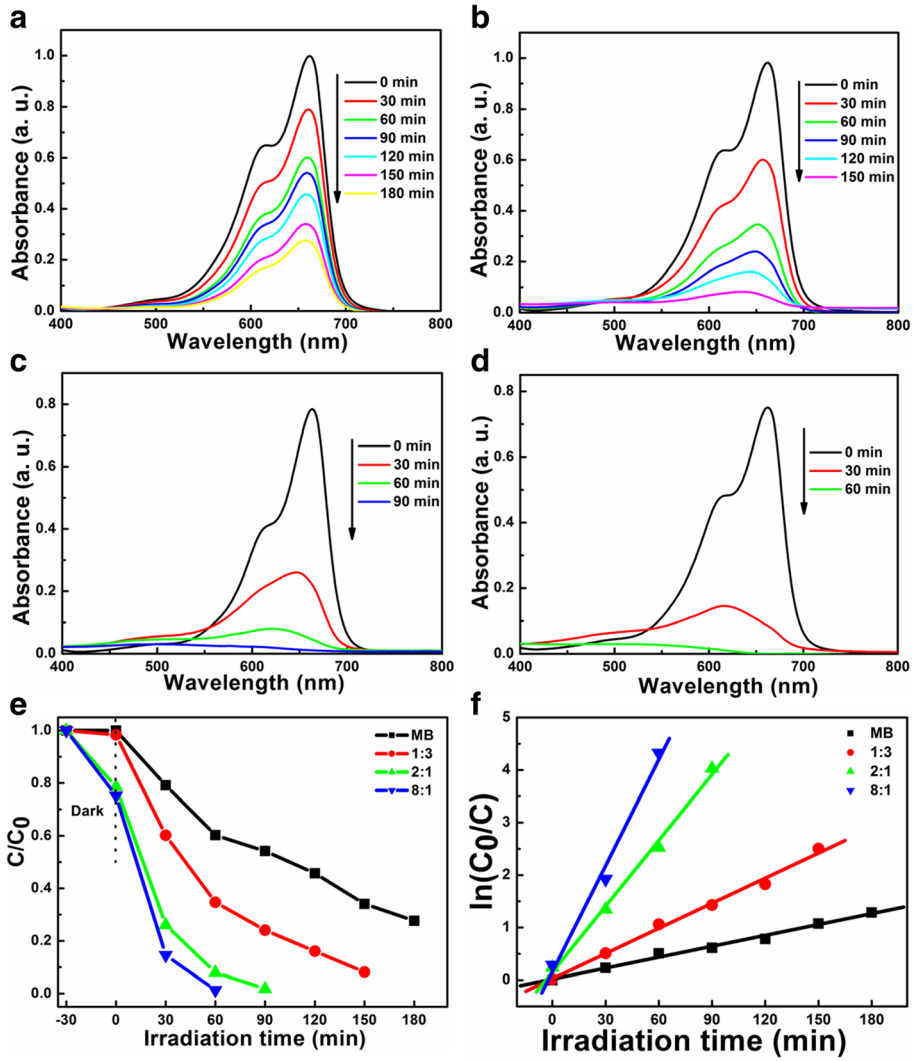

Fig. 8 UV-vis absorption spectra of the degradation of MB: **a** without catalyst and catalyzed by **b** $LiNb_3O_8$-1:3, **c** $LiNbO_3$, and **d** $LiNb_3O_8$-8:1, respectively. **e** Photo-degradation of MB and **f** kinetic fit with respect to the irradiation time using Li-Nb-O powders

outstanding the photocatalytic performance is. The k of $LiNb_3O_8$-8:1 is 9.5 times of MB without catalysts, 4.2 times of $LiNb_3O_8$-1:3, and 1.6 times of $LiNbO_3$. Compared with $LiNb_3O_8$-1:3, the higher photocatalytic performance of $LiNb_3O_8$-8:1 can be attributed to the unique porous and hollow structure, which provides a high density of active sites for the degradation of MB [31].

Compared to $LiNbO_3$, the improved photocatalytic performance of $LiNb_3O_8$-8:1, which has almost the same absorption ability of MB as that of $LiNbO_3$, can be attributed to its layered structure type with the reduce symmetry. The layered structure can enhance the separation of electrons and holes [32], consistent with the PL spectra, as shown in Fig. 9. At the same time, the $LiNb_3O_8$ framework is constructed by three different niobate octahedrons and Li atoms share partial octahedral sites; the higher niobate octahedral site is expected to provide more active sites for photocatalysis. Finally, the smaller energy band gap of $LiNb_3O_8$ (about 3.9 eV) than that of $LiNbO_3$ (4.14 eV) means that it can utilize more incident light to participate in the photocatalytic process [33].

The separation efficiency of photogenerated carries of Li-Nb-O catalyst are investigated by PL spectra, as shown in Fig. 9. As we know, PL emission spectra mainly result from the recombination of free carriers. As seen in Fig. 9, $LiNb_3O_8$ shows smaller emitting peaks around 470 nm than $LiNbO_3$. It means that $LiNb_3O_8$ has longer charge carrier lifetime and improved efficiency of interfacial charge transfer, which can be attributed to its layered structure with the reduced symmetry enhancing the separation of electrons and holes.

Conclusions

From the results above, we can conclude that Li/Nb ratio has a great impact on the formation of $LiNbO_3$; the ratio smaller than 3:1 is beneficial to the formation of $LiNbO_3$, while larger than 3:1, forms no $LiNbO_3$ at all and the morphology and chemical bond of Nb_2O_5 raw material are totally modified by Li ions. The reason can be attributed to the large content of LiOH, which is beneficial to form Li_3NbO_4 not $LiNbO_3$, and also, even if the $LiNbO_3$ particle locally forms, it is easily dissolved in LiOH solution with strong alkalinity. Pure $LiNb_3O_8$ powders are obtained with two absolutely opposite Li/Nb ratios: 8:1 and 1:3; the former shows a unique porous and hollow structure, quite different with the particle aggregation (the latter shows). Compared with Li/Nb = 1:3, higher photocatalytic performance of $LiNb_3O_8$ (Li/Nb = 8:1) are observed and it can be attributed to the unique porous and hollow structure, which provides a high density of active sites for the degradation of MB. Compared to $LiNbO_3$, the improved photocatalytic performance of $LiNb_3O_8$ can be attributed to its layered structure type with the reduced symmetry enhancing the separation of electrons and holes.

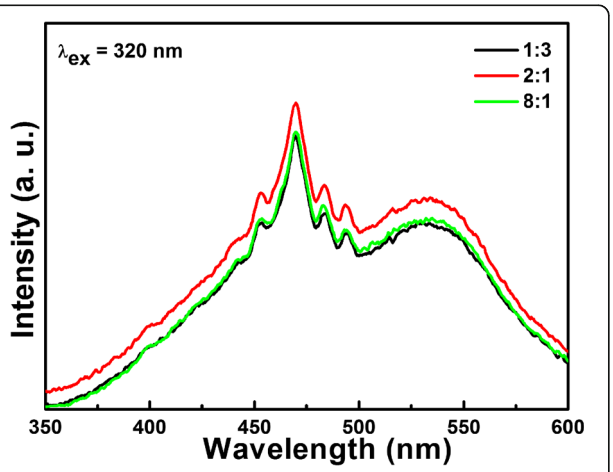

Fig. 9 Room temperature PL spectra of $LiNb_3O_8$-1:3, $LiNbO_3$, and $LiNb_3O_8$-8:1 catalysts

Acknowledgements

This work was financially supported by the National Natural Science Foundation of China (No. 51202107) and the Foundation of Henan Educational Committee (No. 16A140028).

Authors' contributions

HZ and HL conceived and designed the experiments; HL and LZ prepared the samples; CH and ZW performed the XRD and SEM measurements; JQ performed the XPS; JY participated in the photocatalytic test; HZ wrote the paper. All of the authors read and approved the final manuscript.

Competing interests

The authors declare that they have no competing interests.

Publisher's Note

Received: 3 June 2017 Accepted: 11 August 2017
Published online: 15 August 2017

References

1. Nico C, Monteiro T, Graça MPF (2016) Niobium oxides and niobates physical properties: review and prospects. Prog Mater Sci 80:1–37
2. Zhai HF, Li AD, Kong JZ, Li XF, Zhao J, Guo BL, Yin J, Li ZS, Wu D (2013) Preparation and visible-light photocatalytic properties of $BiNbO_4$ and $BiTaO_4$ by a citrate method. J Solid State Chem 202:6–14
3. Zhai HF, Shang SY, Zheng LY, Li PP, Li HQ, Luo HY, Kong JZ (2016) Efficient visible-light photocatalytic properties in low-temperature Bi-Nb-O system photocatalysts. Nanoscale Res Lett 11:383
4. Kumar S, Davila N, Wang ZW, Huang XP, Strachan JP, Vine D, Kilcoyne ALD, Nishi Y, Williams RS (2017) Spatially uniform resistance switching of low current, high endurance titanium-niobium-oxide memristors. Nano 9:1793–1798
5. Abe R, Shinmei K, Koumura N, Hara K, Ohtani B (2013) Visible-light-induced water splitting based on two-step photoexcitation between dye-sensitized layered niobate and tungsten oxide photocatalysts in the presence of a triiodide/iodide shuttle redox mediator. J Am Chem Soc 135:16872–16884
6. Pullar RC (2009) The synthesis, properties, and applications of columbite niobates ($M^{2+}Nb_2O_6$): a critical review. J Am Ceram Soc 92:563–577
7. Janner D, Tulli D, Garcia-Granda M, Belmonte M, Pruneri V (2009) Micro-structured integrated electro-optic $LiNbO_3$ modulators. Laser Photonics Rev 3:301–313
8. Liu JW, Chen G, Li ZH, Zhang ZG (2007) Hydrothermal synthesis and photocatalytic properties of $ATaO_3$ and $ANbO_3$ (A = Na and K). Int J Hydrogen Energ 32:2269–2272

9. Zhai HF, Kong JZ, Wang AZ, Li HJ, Zhang TT, Li AD, Wu D (2015) The polymerization effect on synthesis and visible-light photocatalytic properties of low-temperature β-$BiNbO_4$ using Nb-citrate precursor. Nanoscale Res Lett 10:457
10. Wang X, Yan WB, Zhang LX, Shi LH, Chen HJ, Zhang YW, Wu M, Zhang PJ (2015) Tunable photocatalytic activity of photochromic Fe-Mn-codoped $LiNbO_3$ nanocrystals. Opt Mater Express 5:2240–2245
11. Zhai HF, Liu HR, Li HJ, Zheng LY, Hu CJ, Zhang X, Li QL, Yang JE (2017) Hydrothermal-assisted sintering strategy towards porous- and hollow-structured $LiNb_3O_8$ anode material. Nanoscale Res Lett 12:463
12. Yin J, Zou ZG, Ye JH (2003) Photophysical and photocatalytic properties of $MIn_{0.5}Nb_{0.5}O_3$ (M = Ca, Sr, and Ba). J Phys Chem B 107:61–65
13. Liu JL, Shakir I, Kang DJ (2014) Single crystalline $LiNb_3O_8$ nanoflakes for efficient photocatalytic degradation of organic pollutants. RSC Adv 4:4917–4920
14. Jian ZL, Lu X, Fang Z, Hu YS, Zhou J, Chen W, Chen LQ (2011) $LiNb_3O_8$ as a novel anode material for lithium-ion batteries. Electrochem Commun 13:1127–1130
15. Xu HH, Shu J, Hu XL, Sun YM, Luo W, Huang YH (2013) Electrospun porous $LiNb_3O_8$ nanofibers with enhanced lithium-storage properties. J Mater Chem A 1:15053–15059
16. Liu JL, Shakir I, Kang DJ (2014) Lithium niobate nanoflakes as electrodes for highly stable electrochemical supercapacitor devices. Mater Lett 119:84–87
17. Sahoo PP, Maggard PA (2013) Crystal chemistry, band engineering, and photocatalytic activity of the $LiNb_3O_8$–$CuNb_3O_8$ solid solution. Inorg Chem 52:4443–4450
18. Zielińska B, Borowiak-Palen E, Kalenzuk RJ (2008) Preparation and characterization of lithium niobate as a novel photocatalyst in hydrogen generation. J Phys Chem Solids 69:236–242
19. Debnath C, Kar S, Verma S, Bartwal KS (2015) Synthesis of $LiNbO_3$ nanoparticles by citrate gel method. J Nanosci Nanotechnol 15:3757–3763
20. Sumets M, Kostyuchenko A, Ievlev V, Kannykin S, Dybov V (2015) Influence of thermal annealing on structural properties and oxide charge of $LiNbO_3$ films. J Mater Sci Mater Electron 26:7853–7859
21. Yu J, Liu XQ (2007) Hydrothermal synthesis and characterization of $LiNbO_3$ crystal. Mater Lett 61:355–358
22. Ferreira NM, Ferro MC, Graca MPF, Costa FM (2017) Effect of laser irradiation on lithium niobate powders. Ceram Int 43:2504–2510
23. Ning HX, Liao QL, Xiong J (2009) Study on $LiNbO_3$ ultrafine powders synthesized by hydrothermal method. Piezoelectrics & Acoustooptics 31:103–105
24. Akazawaa H, Shimada M (2007) Mechanism for $LiNb_3O_8$ phase formation during thermal annealing of crystalline and amorphous $LiNbO_3$ thin films. J Mater Res 22:1726–1736
25. Prado AGS, Bolzon LB, Pedroso CP, Moura AO, Costa LL (2008) Nb_2O_5 as efficient and recyclable photocatalyst for indigo carmine degradation. Appl Catal B-Environ 82:219–224
26. Katovic V, Djordjevic C (1970) Coordination complexes of niobium and tantalum. VII. Preparation and infrared spectra of oxygen-18 labeled terminal and bridging monoxoniobium(V) complexes and the course of coordinated alkoxo group hydrolysis in mixed-ligand niobium complexes. Inorg Chem 9:1720–1723
27. Braga VS, Garcia FAC, Dias JA, Dias SCL (2008) Phase transition in niobium pentoxide supported on silica-alumina. J Therm Anal Calorim 92:851–855
28. Bartasyte A, Plausinaitiene V, Abrutis A, Stanionyte S, Margueron S, Boulet P, Kobata T, Uesu Y, Gleize J (2013) Identification of $LiNbO_3$, $LiNb_3O_8$ and Li_3NbO_4 phases in thin films synthesized with different deposition techniques by means of XRD and Raman spectroscopy. J Phys Condens Matter 25:205901
29. Cochez M, Ferriol M, Pöppl L, Polgár K, Péter Á (2005) Ternary system Li_2O–K_2O–Nb_2O_5 part I: phase equilibria around the lithium niobate existence field. J Alloy Compd 386:238–245
30. Al-Ekabi H, Serpone N (1988) Kinetics studies in heterogeneous photocatalysis. I. Photocatalytic degradation of chlorinated phenols in aerated aqueous solutions over titania supported on a glass matrix. J Phys Chem 92:5726–5731
31. Liu J, Xue DF (2008) Thermal oxidation strategy towards porous metal oxide hollow architectures. Adv Mater 20:2622–2627
32. Sabio EM, Chi MF, Browning ND, Osterloh FE (2010) Charge separation in a niobate nanosheet photocatalyst studied with photochemical labeling. Langmuir 26:7254–7261
33. Zlotnik S, Tobaldi DM, Seabra P, Labrincha JA, Vilarinho PM (2016) Alkali niobate and tantalate perovskites as alternative photocatalysts. ChemPhysChem 17:3570–3575